Tilt sensitivity of the two-grating interferometer

Christopher N. Anderson[1,*] and Patrick P. Naulleau[2]

[1] *Applied Science & Technology Graduate Group, University of California at Berkeley, Berkeley, CA 94720, USA*

[2] *Center for X-ray Optics, Lawrence Berkeley National Laboratroy, 1 Cyclotron Road, Berkeley, CA 94720, USA*

[*] *Corresponding author: cnanderson@berkeley.edu*

Fringe formation in the two-grating interferometer is analyzed in the presence of a small parallelism error between the diffraction gratings assumed in the direction of grating shear. Our analysis shows that with partially coherent illumination, fringe contrast in the interference plane is reduced in the presence of nonzero grating tilt with the effect proportional to the grating tilt angle and the grating spatial frequencies. Our analysis also shows that for a given angle between the gratings there is an angle between the final grating and the interference plane that optimizes fringe contrast across the field.

1. Introduction

Many authors have studied the details of fringe formation in the two-grating interferometer [1–7]. To date, however, all of the theory describing fringe formation in the far-field

two-grating interferometer has assumed parallel diffraction gratings. In near-field Talbot interferometry (which also uses two gratings) Patorski [8, 9] and Liu [10, 11] have shown that fringe formation is sensitive to small parallelism errors between the diffraction gratings. It is reasonable to assume that fringe formation in the far-field two-grating interferometer is also sensitive to small grating parallelism errors.

Cheng [6] has shown that the fringe depth of the parallel two-grating interferometer is inversely proportional to the spatial frequency of the gratings and the numerical aperture (NA) of the illumination. It is reasonable to believe that the effects of small grating parallelism errors may also scale inversely with grating spatial frequency and illumination NA. Experimental evidence [12] suggests that when low-NA sources are used, the requirements on grating parallelism are well within the capability of typical alignment stages. On the other hand, for high spatial frequency implementations ($\sim$ 15-nm grating pitch), using higher-NA sources, it is reasonable to suspect that the requirements on grating parallelism might become a significant issue in practice.

Extreme ultraviolet (EUV) lithography is the leading candidate for high-volume chip production beyond the 32-nm technology node [13, 14]. Owing to their low cost, there is currently an interest in developing stand-alone EUV interference lithography (IL) printing tools. Unfortunately, stand-alone coherent sources are not mature enough to support the rapid development of coherent IL tools [16]. To date, the best source options for stand-alone EUV IL tools are incoherent (broad) sources [17]. Due to the large collection NA of these sources and the high grating frequencies required to print features beyond the 32-nm technology node, there are serious concerns about the feasibility of implementing incoherent EUV IL tools in practice.

In this paper we will examine fringe formation in the far-field two-grating interferometer in the presence of a small parallelism error between the diffraction grartings. The goal of this paper is to address the impact of the parallelism error and other experimental uncertainties on fringe formation as a function of illumination NA, spectral bandwidth, center wavelength

and nominal angle of incidence.

2. Previous work on the parallel two-grating interferometer

The parallel two-grating interferometer has been analyzed to several orders of accuracy in the literature. The analysis by Leith et al. [2–4] was based on a first-order approximation of the transfer function of free space. It was found that nonlocalized fringes form for polychromatic plane-wave illumination at any angle θ and localized fringes form for extended sources (multiple illumination angles), regardless of source spectral bandwidth (color content). This work concluded that in defocused interference planes, different illumination angles produce shifted versions of the same fringe pattern with the fringe patterns of all spectral elements (colors) coinciding. The net fringe dephasing between extreme illumination angles in the illumination cone was found to be proportional to the illumination NA and the longitudinal distance from the nominal interference plane.

In follow-up work by Cheng [6], a higher order analysis of the parallel two-grating interferometer was performed using a geometrical ray-tracing approach. This analysis showed that the $f_2 = 2f_1$ case, where f_1 and f_2 are the spatial frequencies of the first and second gratings, respectively, is a special configuration in which many of the second-order terms are mitigated. To second order with the $f_2 = 2f_1$ geometry, it was found that for on-axis illumination, the interference fringes produced by different spectral elements coincide with one another. It was also found that as the illumination angle goes off axis, the interference fringes produced by different spectral elements no longer coincide except in the nominal (zero-defocus) interference plane. The work by Cheng showed both the illumination NA and source spectral bandwidth play a role in fringe localization in the parallel two-grating interferometer.

To study the nonparallel two-grating interferometer we will use a phase tracking technique similar to the transfer function approach used by Leith. Instead of explicitly writing the illumination in terms of spatial frequency content we will leave the incidence angle and illumination wavelength dependence separated so that we can easily study how angle content

and spectral content independently affect the interferometer.

3. Phase tracking framework

The geometry of the two-grating interferometer is shown in Figure 1. The incoming light strikes grating G_1 (spatial frequency f_1, assumed sinusoidal) and splits into three diffracted orders. The ± 1 diffracted orders from G_1 propagate a distance z_1 to grating G_2 (spatial frequency f_2, assumed sinusoidal) where they are redirected back towards the optic axis. The ∓ 1 diffracted orders from G_2 propagate a distance z_2 past the second grating to a interference plane where they may overlap and produce a modulated intensity pattern.

Before we can track the phase of the two beams as they propagate through the nonparallel interferometer we need to derive the propagation phase of free space between nonparallel planes. We also need to work out the diffraction grating phase for non-tilted and tilted gratings. As has been done in the past will ignore diffraction effects from the edges of gratings and apertures [2–7].

3.A. Propagation phase

Consider a plane wave propagating at an angle θ with respect to the optical axis. To determine the phase acquired by the plane wave in propagating an axial distance z_1 we must compare the relative phase of the plane wave at the same transverse point x in the longitudinal planes $z = 0$ and $z = z_1$.

3.A.1. Parallel planes

Let's look at the transverse point $x = 0$ for simplicity. As shown in Figure 2 (left), the point $(x = 0, z = 0)$ lies on the surface of the original wavefront, on axis. The ray reaching the point $(x = 0, z = z_1)$ on G_2, however, comes from an off-axis location on the original wavefront. The ray reaching the point $(x = 0, z = z_1)$ must travel a distance $z_1 \cos\theta$ from the original wavefront surface that was in phase with the $(x = 0, z = 0)$ point. Using this geometry, we determine the propagation phase of free space propagation between two parallel planes [18]:

$$\phi(z,\theta,\lambda) = \frac{2\pi}{\lambda} z\cos\theta \tag{1}$$

where z is the on-axis longitudinal separation between the two planes, θ is the propagation angle with respect to (with respect to) the optic axis and λ is the wavelength.

3.A.2. Tilted planes

For the case of tilted planes we need to look at an off axis x point to observe the effect of the tilt. As shown in Figure 2 (right) the ray reaching the x coordinate of the tilted G_2 plane (the solid line) comes from a different location on the original wavefront than the ray reaching the same x coordinate of the non-tilted G_2 plane (the dashed line). The grating tilt angle g causes the ray to travel an extra tilt-induced distance $x\tan g\cos\theta$ in addition to the distance $z_1\cos\theta$ traveled in the parallel configuration. This extra path length lends itself to a nice physical picture, namely, the notion of an x dependent axial distance:

$$z_1'(x) = z_1 + x\tan g \tag{2}$$

By including the possibility of a tilt in the first plane, we develop the propagation phase of free space propagation between two tilted planes:

$$\phi(z,\theta,\lambda) = \frac{2\pi}{\lambda}(z - x\tan\theta_1 + x\tan\theta_2)\cos\theta \tag{3}$$

where $\theta_{1,2}$ are the tilt angles of planes 1 and 2 relative to the normal of the optic axis, θ is the propagation angle with respect to the optic axis, and z is the on-axis longitudinal separation between planes 1 and 2. The two x dependent terms are understood as tilt corrections to the propagation phase.

3.B. Grating phase

It is well known [19] that diffraction gratings add a linear phase $\phi(x) = 2\pi m f x$ to the outgoing (diffracted) field where f and m are the grating spatial frequency and diffraction

order, respectively . To correctly use this phase, however, the incoming field distribution must be written in the coordinate system whose optic axis is normal to the grating plane. Our geometry poses a problem for nonzero grating tilt g because in these configurations the field will be written in a coordinate system whose optic axis is tilted with respect to the grating normal. Nevertheless it is not very difficult to develop the framework to correctly describe the effect of grating phase with our geometry.

By definition, the grating phase is simply the phase difference between the field just before and just after the grating surface. Consider a plane wave propagating at an angle θ with respect to the optic axis (which we define as the normal to G_1) and impinging on G_2. For the non-tilted case (Figure 3 left), as you move away from the optical axis along the surface of the grating, you observe light that has travelled a distance $x \sin\theta$ further than the light that strikes the grating at the optical axis. If we tilt the grating (Figure 3 right) by an angle g and keep the same observation coordinate x, we observe that the light reaching the grating travels an extra tilt-induced distance $x \tan g \cos\theta$ in addition to the original distance $x \sin\theta$ traveled in the non-tilted configuration. Using these geometric distances we determine the phase (ϕ) of the field on the front surface of the grating as a function of the transverse distance x from the optical axis.

$$\phi_{front}(x) = \frac{2\pi}{\lambda} x(\sin\theta_{in} + \tan g \cos\theta_{in}) \tag{4}$$

where θ_{in} is the incoming propagation angle with respect to the optic axis. We can also compute the phase of the field on the rear surface of the grating using similar arguments:

$$\phi_{rear}(x) = \frac{2\pi}{\lambda} x(\sin\theta_{out} + \tan g \cos\theta_{out}) \tag{5}$$

where θ_{out} is the outgoing propagation angle with respect to the optic axis. The phase difference between the field at the front and rear surfaces of the grating, the grating phase, is given by:

$$\phi_g(x) = \phi_{rear} - \phi_{front} = \frac{2\pi}{\lambda} x \left[\sin\theta_{out} - \sin\theta_{in}\right] + \frac{2\pi}{\lambda} x \tan g \left[\cos\theta_{out} - \cos\theta_{in}\right] \qquad (6)$$

To compute θ_{out} we use the grating equation:

$$\theta_{out} = \arcsin\left[\sin(\theta_{in} + g) + m\lambda f\right] - g \qquad (7)$$

where f is the grating spatial frequency, m is the diffraction order and it is understood that we transfer into a coordinate system normal to the grating surface, use the standard grating equation [20], and then transfer back to the original coordinate system. With this propagation phase and grating phase framework we can now propagate a plane wave through the two-grating interferometer for arbitrary illumination angles, grating frequencies, axial distances and grating tilts.

4. Propagation through the interferometer

We now set out to determine the intensity distribution in the overlap region for arbitrary $\theta,\ \lambda,\ f_1,\ f_2,\ ,z_1,\ z_2,\ g$ and interference plane tilt w. For bookkeeping purposes we will break the two-grating interferometer into two regions: 1 and 2; and two beams: top (T) and bottom (B) as shown in Figure 4. As an example of the nomenclature we write $\sin\theta_{T2}$ for the sin of the propagation angle of the top (T) beam in region 2. The optic axis will be defined as the normal to the surface of G_1 so that all grating tilts are absorbed into G_2. The grating phase assigned to a region will be the grating phase from the diffraction grating at the beginning of the region, i.e., region 1 is assigned the grating phase from G_1. The prescription for tracking the phase of a beam through the nonparallel two-grating interferometer is as follows:

1. Input a monochromatic (wavelength λ) unit amplitude plane wave propagating at angle θ with respect to the optic axis.

2. Apply grating phase for non-tilted G_1

3. Apply propagation phase for propagating the axial distance z_1 at angle θ_1 between non-tilted G_1 and tilted G_2

4. Apply grating phase for tilted G_2

5. Apply propagation phase for propagating the axial distance z_2 at angle θ_2 between tilted G_2 and tilted interference plane

The fields of the top and bottom beams in the tilted interference plane can be used to compute the intensity pattern created by the input plane wave:

$$\begin{aligned} I(x) = |E_T + E_B|^2 &= |E_T|^2 + |E_B|^2 + E_T E_B^* + E_T^* E_B \\ &= 2 + 2\cos\left(\phi(x, \theta,\ \lambda,\ f_1,\ f_2,\ z_1,\ z_2,\ g,\ w)\right) \end{aligned}$$

where $\phi = \phi_T - \phi_B$ is the phase difference between the top and bottom beams in the tilted interference plane; we will omit the explicit $x,\ \theta,\ \lambda,\ f_1,\ f_2,\ ,z_1,\ z_2,\ g,\ w$ dependence from here on out. Tables 1 and 2 summarize the propagation phase and grating phase, respectively, acquired by each beam during propagation through the two-grating interferometer. To determine the propagation angles of the top and bottom beams in regions 1 and 2 we use Eq. (7):

$$\begin{aligned} \theta_{T1} &= \arcsin\left[\sin\theta + \lambda f_1\right] \\ \theta_{B1} &= \arcsin\left[\sin\theta - \lambda f_1\right] \\ \theta_{T2} &= \arcsin\left[\sin(\theta_{T1} + g) - \lambda f_2\right] - g \\ \theta_{B2} &= \arcsin\left[\sin(\theta_{B1} + g) + \lambda f_2\right] - g \end{aligned} \tag{8}$$

When computing the phase difference ϕ between the top and bottom beams in the tilted interference plane, all of the terms explicitly involving the G_2 tilt (g) cancel; the influence of the grating tilt remains buried inside the terms containing region 2 propagation angles.

$$\phi = \frac{2\pi}{\lambda} z_1 C_1 + \frac{2\pi}{\lambda}(z_2 + x\tan w)C_2 + \frac{2\pi}{\lambda} x S_2 \tag{9}$$

where

$$C_1(\lambda,\ \theta,\ f_1) = \cos\theta_{T1} - \cos\theta_{B1}$$

$$C_2(\lambda,\ \theta,\ f_1,\ f_2) = \cos\theta_{T2} - \cos\theta_{B2}$$

$$S_2(\lambda,\ \theta,\ f_1,\ f_2) = \sin\theta_{T2} - \sin\theta_{B2}$$

5. Revealing the impact of the grating tilt

Up to this point, there have been no approximations except that we have ignored diffraction effects from the edges of the gratings and apertures. In an attempt to unmask the implicit effect of the G_2 tilt buried in ϕ we now set out to simplify the troublesome terms involving the region 2 propagation angles governed by Eq. (7). We begin by introducing the notion of an effective spatial frequency f_2' for G_2 in the presence of a small tilt g. That is, we wish to create a virtual non-tilted grating G_2' with frequency f_2' that generates the same propagation angles as the true tilted G_2 at spatial frequency f_2. Assuming a small grating tilt allows us to use the expansion:

$$\arcsin(\alpha + \delta) \approx \arcsin\alpha + \delta(1-\alpha^2)^{-1/2} \tag{10}$$

on Eq. (7) to pull the grating tilt *inside* the arcsin argument, i.e.,

$$\theta_{out} \approx \arcsin\left[\sin(\theta_{in} + g) + m\lambda f - g\left(1 - [\sin(\theta_{in} + g) + m\lambda f]^2\right)^{1/2}\right]$$

Furthermore, since small g is assumed, we can make another expansion, namely:

$$\sin(\theta_{in} + g) \approx \sin\theta_{in} + g\cos\theta_{in}$$

so that Eq. (7) is well approximated by:

$$\theta_{out} \approx \arcsin\left[\sin\theta_{in} + m\lambda f'\right] \tag{11}$$

where

$$f' = f + \frac{g}{m\lambda}\left[\cos\theta_{in} - \left(1 - \left[\sin\theta_{in} + g\cos\theta_{in} + m\lambda f\right]^2\right)^{1/2}\right]$$

is the effective spatial frequency of the virtual grating (a function of f, λ, g, θ_{in} and m).

Continuing our efforts to unmask the effect of the G_2 tilt, we will now assume several restrictions on the interferometer geometry that make the problem tractable. As described by Cheng [6], the $f_2 = 2f_1$, $z_1 = z_2$ configuration of the parallel two-grating interferometer is a special case in which many of the second-order spectral bandwidth and angle bandwidth terms drop out. For the remainder of our analysis we will consider practical implementations of this configuration and assume $f_2 = 2f_1(1+\gamma)$ and $z_2 = z_1 + d$ where γ is understood as a small unitless G_2 pitch error and d is a small defocus parameter. With this configuration, it can be shown (see Appendix A) that the effective spatial frequency of G_2' for both beams (top and bottom) is well approximated by:

$$f_2' = 2f_1(1+\gamma) - \frac{g}{\lambda}C_1$$

Using the notion of the virtual non-tilted G_2' we can use Eq. (11) with the above f_2' to write approximate expressions for the region 2 propagation angles that were originally obtained with Eq. (7) .

$$\theta_{T1} = \arcsin\left[\sin\theta + \lambda f_1\right]$$

$$\theta_{B1} = \arcsin\left[\sin\theta - \lambda f_1\right]$$

$$\theta_{T2} \approx \arcsin\left[\sin\theta_{B1} - 2\lambda f_1\gamma + gC_1\right]$$

$$\theta_{B2} \approx \arcsin\left[\sin\theta_{T1} + 2\lambda f_1\gamma - gC_1\right] \tag{12}$$

To simplify the C_2 term with the rewritten propagation angles we introduce the expansion:

$$\cos\left[\arcsin(\sin\alpha + \delta)\right] \approx \cos\alpha - \delta\tan\alpha - \frac{\delta^2}{2\cos^3\alpha} \tag{13}$$

where we have expanded the function $f(x) = \cos\left[\arcsin(x)\right] = (1 - x^2)^{1/2}$ to second order about the nominal value $\sin\alpha$ and have assumed δ is a small correction term. Using Eq. (13) to expand C_2 to first order in the small parameters g and γ we obtain:

$$C_2 \approx -C_1 + (2\lambda f_1\gamma - gC_1)\,T_1$$

where:

$$T_1(\lambda,\ \theta,\ f_1) = \tan\theta_{T1} + \tan\theta_{B1}$$

Simplifying the S_2 term in Eq. (9) is relatively straightforward with the new propagation angles from Eq. (12); the result is $S_2 \approx -2f_1(1 + 2\gamma)/\lambda$. Combining all of these approximations we achieve an expression for the phase that explicitly shows the impact of G_2 tilt and pitch error:

$$\phi \approx -\underbrace{2\pi x(2f_1)(1+2\gamma)}_{\text{desired modulaiton}} + \underbrace{2\pi x/\lambda\left[2gC_1 + \tan w\left(-C_1 + 2\lambda f_1 \gamma T_1 - gC_1T_1\right)\right]}_{\text{unwanted modulation}}$$
$$+ \underbrace{2\pi/\lambda\left[-dC_1 + z_1\left(2\lambda f_1\gamma - gC_1\right)T_1\right]}_{\theta,\,\lambda \text{ dependent fringe shift}}$$

Regarding the unwanted modulation term, it can be shown that when the interference plane tilt, w, is exactly twice the grating tilt, g, all first order terms in small parameters g and γ cancel leaving only terms of $\mathcal{O}(2)$ and higher in the small parameters. For the remainder of the analysis we will assume that $w = 2g$ and drop the unwanted modulation term. Any remaining interference plane tilt error with respect to the nominal tilt of $2g$ can be lumped into a transversely varying defocus. The expression for the phase becomes:

$$\phi \approx -d\left[2\pi C_1/\lambda\right] + \gamma\left[4\pi z_1 f_1 T_1\right] - g\left[2\pi z_1 C_1 T_1/\lambda\right] - 2\pi x(2f_1)(1+2\gamma) \tag{14}$$

and we remind the reader that C_1 and T_1 are both functions of θ, λ, and f_1. The first and last terms in this expression represent the usual defocus term described in detail in the literature [6,7] and the desired modulation at spatial frequency $2f_1(1+2\gamma)$, respectively. The second and third terms represent γ and g induced limitations, respectively, on the tolerable illumination $\Delta\theta$ and $\Delta\lambda$ that maintain fringe contrast in the interference plane – even with zero defocus.

6. Discussion

We begin by reminding the reader that the analysis leading to Eq. (14) extends only to the limited class of two-grating interferometers with small tilts between the gratings and with $z_2 \approx z_1$ and $f_2 \approx 2f_1$. In this special configuration we've obtained an expression for the phase ϕ that explicitly shows the effects of grating tilt, pitch mismatch and interference plane defocus.

The utility of the interferometer, however, doesn't depend on the phase itself, but how rapidly it changes as a function if illumination color and angle. For nonzero g, γ and d, the first three terms in Eq. (14) independently cause dephasing between the fringe patterns associated with different illumination colors and angles. To have an interferometer in working order (i.e., having reasonable fringe contrast) the fringe-pattern-shift from the two extreme illumination spatial frequencies should be less than the width of a fringe. Satisfying this specification requires the net dephasing from the first three terms in Eq. (14) to be less than π.

6.A. Illumination conditions

At this point it is useful to define two illumination classes that limit fringe contrast in clear-cut ways:

1. Temporally limiting illumination
    - Polychromatic with bandwidth $\Delta\lambda$ and center wavelength $\bar{\lambda}$ (partially temporally coherent).
    - One incidence angle at θ_0 (spatially coherent)
2. Spatially limiting illumination
    - Monochromatic at wavelength $\bar{\lambda}$ (temporally coherent).
    - Full-NA of incidence angles $\Delta\theta$ centered at θ_0 (partially spatially coherent).

For temporally limiting illumination in the ideal configuration ($g = \gamma = 0$) it has been shown [6, 7] that the temporal-limited depth of focus is given by:

$$DOF_{\Delta\lambda} = \frac{\cos^4\theta_0}{2\bar{\lambda}\Delta\lambda f_1^3 \tan\theta_0} \tag{15}$$

where the DOF is defined as the twice the largest d that limits the net dephasing from different colors in the illumination to a maximum value of π (term 1 in Eq. (14)) . In a

similar fashion (see Appendix B) a spatially-limited DOF can be obtained for the ideal configuration ($g = \gamma = 0$) with spatially limiting illumination:

$$DOF_{\Delta\theta} = \frac{\cos^2\theta_0}{2f_1\Delta\theta} \tag{16}$$

When $\Delta\theta$ and $\Delta\lambda$ are both nonzero, the above expressions are useful for determining whether or not one form of dephasing dominates the other; this is often the case in practice. We define the illumination to be NA-limited when the dephasing from illumination spectral content ($\Delta\lambda$) is negligible in comparison to the dephasing from illumination angle content ($\Delta\theta$). The specification requires $DOF_{\Delta\theta} \ll DOF_{\Delta\lambda}$ or:

$$\frac{\Delta\lambda}{\bar{\lambda}} \ll \frac{\Delta\theta\cos^2\theta_0}{(\bar{\lambda}f_1)^2\tan\theta_0} \tag{17}$$

When broad source illumination is used, the illumination is often NA-limited. For example, when $\Delta\theta = 4°$ (0.07 rad), $\theta_0 = 15°$ and $\bar{\lambda}f_1 = 0.25$, NA-limitation requires $\Delta\lambda/\bar{\lambda} \ll 3.9$ which is satisfied by almost any existing source at any center wavelength. Although we've argued this case for the ideal configuration, is reasonable to assume that these characteristics also hold in the $g \neq 0$, $\gamma \neq 0$ configuration. For the remainder of the discussion we will consider the class of nonparallel interferometers that operate in the NA-limited regime: this enables us to treat the specific case of spatially limiting illumination and apply the results to the larger context of all NA-limited illumination schemes. We now focus our attention on Eq. (14), specifically, we wish to determine how θ_0, $\Delta\theta$, g, γ, and d affect fringe formation.

6.B. Grating parallelism tolerances

Before we examine the interplay between the various terms in Eq. (14) we will approximate C_1 and T_1 with Eq. (13) and with the following expansion:

$$\tan[\arcsin(\sin\alpha + \delta)] \approx \tan\alpha + \frac{\delta}{\cos^3\alpha} + \frac{3\delta^2\sin\alpha}{2\cos^5\alpha} \tag{18}$$

Here we have expanded the function $f(x) = \tan[\arcsin(x)] = x/(1-x)^{1/2}$ to second order about the nominal value $\sin\alpha$ and have assumed δ is a small correction term. Using Eqs. (13) and (18) we obtain:

$$\begin{aligned} C_1 &\approx -2\lambda f_1 \tan\theta \\ T_1 &\approx 2\tan\theta + \frac{3\lambda^2 f_1^2 \sin\theta}{\cos^5\theta} \end{aligned} \tag{19}$$

where for small θ the first term in Eq. (19) for T_1 suffices for calculation purposes. With these approximations the various terms in Eq. (14) become easier to analyze.

The first term in in Eq. (14) has already been analyzed in this paper as well as in the literature [6, 7]. The third term in Eq. (14) is unique to the case of nonparallel diffraction gratings and requires some discussion. Using the expressions in Eq. (19) to approximate the C_1T_1 product as $-4\lambda f_1 \tan^2\theta$, we observe that grating tilt (which shows up entirely in term 3) causes different illumination angles to produce different phased (spatially shifted) fringe patterns. For spatially limiting illumination, the dephasing between the extreme angles in the illumination cone is (to first order) proportional to g, f_1, z_1 and $\Delta\theta$ and increases substantially as θ_0 moves off-axis. To visualize the θ_0 dependence, Figure 5 shows the C_1T_1 product and it's derivative for several values of $\eta \equiv \lambda f_1 \in [0.05, 0.25]$ with $-45 < \theta < 45$ degrees. These plots clearly show that the local slope of C_1T_1 increases nonlinearly from zero as θ_0 moves off-axis.

To come up with a tolerance spec on g that enables a workable DOF we require that the dephasing caused by the grating tilt term in Eq. (14) (term 3) is much less than the dephasing caused by the DOF term (term 1). We first consider the case of an illumination cone centered on-axis, with no grating pitch mismatch ($\gamma = 0$). For illumination with full-NA $\Delta\theta$ and $\theta_0 = 0°$ the dephasing requirement leads to the following condition [23]:

$$g \ll \frac{2d}{z_1 \Delta\theta} = \frac{1}{f_1 z_1 (\Delta\theta)^2} \tag{20}$$

As an example, we consider parameters suitable for an incoherent EUV IL tool: $1/f_1 = 30$ nm, $z_1 = 20$ mm and $\Delta\theta = 4°$. These parameters require $g \ll 300$ μrad which is manageable in practice. As the nominal illumination angle moves off-axis, parallelism tolerances get tighter. The local slopes of C_1T_1 and C_1 can be approximated by:

$$\begin{aligned} \frac{\partial(C_1T_1)}{\partial\theta} &\approx -\frac{8\lambda f_1 \sin\theta}{\cos^3\theta} - \frac{12\lambda^3 f_1^3 \sin\theta}{\cos^7\theta}\left(\cos^2\theta + 3\sin^2\theta\right) \\ \frac{\partial C_1}{\partial\theta} &\approx -\frac{2\lambda f_1}{\cos^2\theta} \end{aligned} \tag{21}$$

where for $\theta < 30°$ the first term in Eq. (21) for C_1T_1 suffices for calculation purposes. To determine the new spec for tolerable g in off-axis geometries we require:

$$z_1 g \Delta\theta \left[\frac{\partial(C_1T_1)}{\partial\theta}\right]_{\theta=\theta_0} \ll d\Delta\theta \left[\frac{\partial C_1}{\partial\theta}\right]_{\theta=\theta_0} \tag{22}$$

Using Eq. (21) (only the first terms) we can solve for g:

$$g \ll \frac{d}{4z_1 \tan\theta_0} = \frac{\cos^3\theta_0}{8 f_1 z_1 \Delta\theta \sin\theta_0} \tag{23}$$

Eq. (23) is equivalent to Eq. (20) with $\Delta\theta$ replaced by $8\tan\theta_0$. With the EUV IL tool parameters form above we find that $\theta_0 = 5°$ requires $g \ll 30$ μrad; increasing θ_0 to $30°$ tightens the spec even more to $g \ll 5$ μrad. These findings suggest that interferometers operating in the NA-limited regime should avoid off-axis implementations (which would be required if reflective gratings are used), especially in applications where high spatial frequency gratings and larger numerical apertures are used.

6.C. Grating pitch mismatch and optimization

Up to this point we have assumed that γ, the grating pitch mismatch, is zero. We now include the possibility of a grating pitch mismatch, however, we treat it in the sense that the pitch mismatch is fixed at one value and cannot be altered. Because g and d can be manipulated in practice, there is the possibility of using a nominal defocus and/or grating tilt to partially mitigate the effects of the pitch mismatch.

One straightforward optimization scheme is to use the dephasing from a small amount of defocus to mitigate most of the dephasing due to the grating pitch mismatch. For this optimization we use term 1 to cancel term 2 in Eq. (14) at the center wavelength and center illumination angle. The optimized value for the defocus is $d_{ideal} = 2z_1\bar{\lambda}f_1\gamma T_1(\theta_0,\ \bar{\lambda})/C_1(\theta_0,\ \bar{\lambda})$. In order to include the possibility of a focus error, now with respect to d_{ideal}, we redefine the defocus parameter: $d \equiv d_{ideal} + d'$ where d' is understood as the defocus with respect to to d_{ideal}. The expression for the phase in this optimization is written:

$$\phi \approx -\frac{2\pi}{\lambda}d'C_1 + 2\pi z_1 2f_1\gamma N - \frac{2\pi}{\lambda}z_1 g C_1 T_1 - 2\pi x(2f_1)(1+2\gamma) \tag{24}$$

where

$$N(\theta,\ \lambda,\ \theta_0,\ \bar{\lambda}) = \left[1 - \frac{\bar{\lambda}T_1(\theta_0,\ \bar{\lambda})C_1(\theta,\ \lambda)}{\lambda T_1(\theta,\ \lambda)C_1(\theta_0,\ \bar{\lambda})}\right] T_1(\theta,\ \lambda)$$

describes the γ-dephasing that could not be cancelled with defocus. For the remainder of the discussion we will drop the prime on d'. Assuming spatially limiting illumination we can simplify the expression for N with the substitution $\lambda \equiv \bar{\lambda}$. In section 6.B we concluded that off-axis implementations should be avoided in applications with large NA's and high grating frequencies; we limit our discussion of pitch mismatch tolerances to illumination cones centered on-axis. When $\theta_0 = 0°$ we can use Eq. (19) to write a very good approximation for N.

$$\underset{\theta_0=0}{N(\theta,\ \lambda)} \approx \frac{3\lambda f_1 C_1}{2}\left(1-\cos^{-4}\theta\right) \approx -3\lambda f_1 C_1 \theta^2$$

where the final approximation is valid only for small θ. A workable DOF requires that the dephasing caused by the remaining pitch mismatch term in Eq. (24) (term 2) is much less than the dephasing caused by the DOF term (term 1). The dephasing requirement leads to the following condition:

$$\gamma \ll \frac{d}{6\lambda^2 f_1^2 z_1 (\Delta\theta)^2} = \frac{1}{24\lambda^2 z_1 (f_1 \Delta\theta)^3} \tag{25}$$

For the EUV IL tool example with $1/f_1 = 30$ nm, $z_1 = 20$ mm, $\Delta\theta = 4°$ and $\lambda = 13.5$ nm, Eq. (25) requires $\gamma \ll 10^{-2}$ or a pitch mismatch much less than one part in a hundred. As the nominal operation wavelength increases and the illumination NA decreases this spec becomes more lenient. We remind the reader that the specification determined here is for the straightforward optimization scheme where defocus dephasing is used to compensate for pitch mismatch dephasing. The optimization parameter space, however, is quite large as it contains three interrelated parameters θ_0, g, and d; determining the optimal combination of g and d for each θ_0 would require a detailed numerical study that will not be pursued in this work.

7. Summary

By using a two-dimensional phase tracking approach we have obtained the exact expression for the interference pattern in a two-grating interferometer when the angle between the gratings (g) and the angle between the final grating and the interference plane is arbitrary. When practical implementations of the $f_2 = 2f_1$, $z_2 = z_1$ configuration are considered and small g is assumed, several binomial expansions of the arguments inside the cosine function of the fringe pattern bring out the wavelength and incidence-angle dependence of grating tilt, grating pitch mismatch, interference plane tilt, and interference plane defocus.

For on-axis and off-axis nominal incidence angles we have derived specifications for tolerable g. It was found that for off-axis nominal incidence angles the specification for tolerable g can become 1 or 2 orders of magnitude more strict than the specification for $\theta_0 = 0°$. In general, the g-induced dephasing is proportional to g, f_1, z_1 and $\Delta\theta$ and increases substantially as θ_0 moves off-axis. For tilt angle g between the two gratings, we have found the optimal angle between the final grating and the interference plane is also g. In this configuration all unwanted modulation terms are of $\mathcal{O}(2)$ or higher in the small parameters g, γ, and d.

It was found that for a small grating pitch mismatch [we assume $f_2 = 2f_1(1+\gamma)$], nonzero nominal defocus and grating tilt may be used to partially mitigate the pitch mismatch dephasing in broad-source implementations. In the straightforward optimization scheme where dephasing from defocus is used to mitigate dephasing form pitch mismatch, a specification for tolerable pitch mismatch has been obtained.

The work presented here has shown that experimental limitations in grating alignment, grating pitch matching and interference plane focus control have an increasingly significant impact on interferometer performance as the grating period decreases and the illumination NA increases. For incoherent EUV IL tools it is clear that off-axis reflection-based implementations should be avoided due to the impractical tolerance on grating alignment. The operation of on-axis transmission-based incoherent EUV IL tools, however, appears to be within the capabilities of existing alignment stages and nano-fabrication facilities.

This research was supported by the NSF EUV Engineering Research Center and was performed at Lawrence Berkeley National Laboratory, which is operated under the auspices of the Director, Office of Science, Office of Basic Energy Science, of the US Department of Energy under Contract No. DE-AC02-05CH11231.

Appendix

A. Effective grating frequency

Starting with Eq. (11):

$$f' = f + \frac{g}{m\lambda}\left[\cos\theta_{in} - \left(1 - [\sin\theta_{in} + g\cos\theta_{in} + m\lambda f]^2\right)^{1/2}\right]$$

we wish to determine f'_{2T}, the effective spatial frequency of the virtual grating G'_2 for the top beam. We make the following substitutions in Eq. (11): $f = 2f_1(1+\gamma)$, $m = -1$, and $\sin\theta_{in} = \sin\theta_{T1} = \sin\theta + \lambda f_1$. We obtain:

$$f'_{2T} = 2f_1(1+\gamma) - \frac{g}{\lambda}\left[\cos\theta_{T1} - \left(1 - [\sin\theta_{B1} + g\cos\theta_{T1} - 2\lambda f_1\gamma]^2\right)^{1/2}\right]$$

where we've used $\sin\theta - \lambda f_1 = \sin\theta_{B1}$ inside the small-bracketed term. As we're only interested in keeping terms that are first order in the small parameters g and γ, we drop the $g\cos\theta_{T1} - 2\lambda f_1\gamma$ term before the squaring operation; we're able to do this because of the preceding g that multiplies everything inside of the large brackets. After simplification we obtain:

$$f'_{2T} \approx 2f_1(1+\gamma) - \frac{g}{\lambda}\left[\cos\theta_{T1} - \cos\theta_{B1}\right]$$

where the bracketed term is equivalent to C_1. The calculation for f'_{2B} (the effective spatial frequency of the virtual grating G'_2 for the bottom beam) is done in a similar fashion and yields the exact same result.

B. Spatially-limited D.O.F.

Starting with:

$$C_1 = \cos\theta_{T1} - \cos\theta_{B1}$$

we can use Eq. (13) to second order [22] to obtain:

$$C_1 \approx -2\lambda f_1 \tan\theta$$

With this approximation for C_1 we can differentiate with respect to θ to obtain:

$$\frac{\partial C_1}{\partial \theta} \approx -\frac{2\lambda f_1}{\cos^2\theta}$$

Using the above relationship, we can determine the value of d where the net dephasing (fringe-pattern-shift) of all the incidence angles within the illumination cone reaches a maximum value of π.

$$\Delta\phi = -d\frac{2\pi}{\lambda}\Delta\theta\left[\frac{\partial C_1}{\partial\theta}\right]_{\theta=\theta_0} = \pi$$

Defining the DOF as twice the maximum dephasing distance, we obtain:

$$DOF_{\Delta\theta} = 2d = \frac{\cos^2\theta_0}{2f_1\Delta\theta}$$

where $\Delta\theta$ is the illumination full numerical aperture (NA) and θ_0 is the nominal illumination angle.

References

1. F. J. Weinberg and N. B. Wood, "Interferometer based on four diffraction gratings," J. Sci. Instrum. 36, 227-230 (1959).
2. E. N. Leith and B. J. Chang, "Space-invariant holography with quasicoherent light," Appl. Opt. 12, 1957-1963 (1973).
3. E. N. Leith and B.J. Chang, "Image Formation with an Achromatic Interferometer," Opt. Commun. 23, 217 (1977)
4. B. J. Chang, R. C. Alferness, and E.N. Leith, "Space-Invariant Achromatic Grating Interferometers: Theory," Appl. Opt. 14, 1592 (1975).

5. B. J. Chang, "Grating-Based Interferometers," Ph.D. Dissertation, U. Michigan (1974). University Microfilm 74-23-170.

6. Y. S. Cheng, "Fringe formation in incoherent light with a two-grating interferometer," Appl. Opt. 23, 3057-3059 (1984).

7. Y. S. Cheng, "Temporal coherence requirement in a symmetric-path grating interferometer," Appl. Opt. 36, 800-804 (1997).

8. K. Patorski, "Talbot interferometry with increased shear," Appl. Opt. 24, 4448-4453 (1985).

9. K. Patorski, "Talbot interferometry with increased shear: further considerations," Appl. Opt. 25, 1111-1116 (1986).

10. Q. Liu and Ryoji Ohba, "Effects of unparallel grating planes in Talbot interferometry," Appl. Opt. 38, 4111-4116 (1999).

11. Q. Liu and Ryoji Ohba, "Effects of unparallel grating planes in Talbot interferometry II," Appl. Opt. 39, 2084-2090 (2000).

12. M. Wei, E. Gullikson, J.H. Underwood, T.K. Gustafson, and D.T. Attwood, "White-light spatial frequency multiplication using soft x-rays," Proc. of SPIE Vol. 2516, 233-239 (1995).

13. . H. Meiling, et. al, First performance results of the ASML alpha demo tool, Proc. SPIE 6151, 615108 (2006).

14. M. Miura, K. Murakami, K. Suzuki, Y. Kohama, Y. Ohkubo, T. Asami, Nikon EUVL development progress summary, Proc. SPIE 6151, 615105 (2006).

15. B. Wu and A. Kumar, "Extreme ultraviolet lithography: A review," J. Vac. Sci. Technol. B 25(6), Nov/Dec 2007.

16. S. Heinbuch, M. Grisham, D. Martz, and J.J. Rocca, Demonstration of a desk-top size high repetition rate soft x-ray laser, Optics Express, 13, 4050, (2005).

17. Stephen F. Horne, Matthew M. Besen, Donald K. Smith, Paul A. Blackborow, Robert DAgostino, Application of a high-brightness electrodeless Z-pinch EUV source for metrol-

ogy, inspection, and resist development, Proc. SPIE 6151, (2006).

18. J. Goodman, "Introduction to Fourier Optics Second Edition," Eq. 3-74. McGraw-Hill, New York, 1968. We note that we have written the propagation phase in terms of angle and wavelength rather than in terms of spatial frequency as done by Goodman. It is for this reason we do not call call the propagation phase a transfer function. We also note that this phase is exact; the Fresnel approximation has not yet been made.
19. J. Goodman, "Introduction to Fourier Optics Second Edition," Sec 4.5.2. McGraw-Hill, New York, 1968.
20. E. Hecht, "Optics Third Edition," Eq. 10.61. Addison-Wesley Longman, U.S. 1998.
21. Here the 'small correction term' contains the small grating tilt parameter g so a first order expansion is reasonable.
22. Here the 'small correction term' does not contain a small parameter (g, γ, d) so we go to second order to maintain reasonable accuracy in the expansion.
23. Because the DOF dephasing term is odd in theta we need to use the full NA ($2\Delta\theta$) to get the full dephasing for the DOF term. The tilt dephasing term is even in theta so only the half NA is required here.

List of Figures

List of Tables

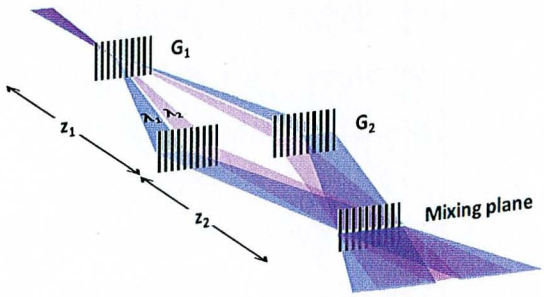

Fig. 1. The two-grating interferometer. All diffraction gratings are assumed sinusodial. For instructive purposes, the illumination contains two distinct wavelengths, λ_1 and λ_2, in a small numerical aperture (NA) of incidence angles centered on-axis. It is assumed the zero-order transmitted beam is blocked at the second grating so it is not shown. Darker shades indicate locations where the two distinct colors spatially overlap.

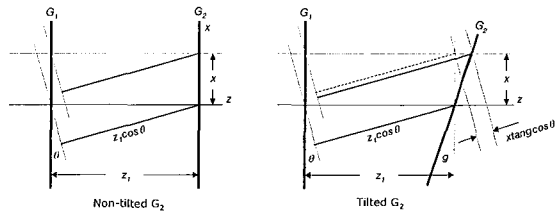

Fig. 2. Computing the propagation phase of free space. This is a side-view schematic of the two-grating interferometer in non-tilted (left) and tilted (right) configurations. The dashed line in the tilted case shows the ray that is used for the non-tilted case. See section 2.A for an in-depth description.

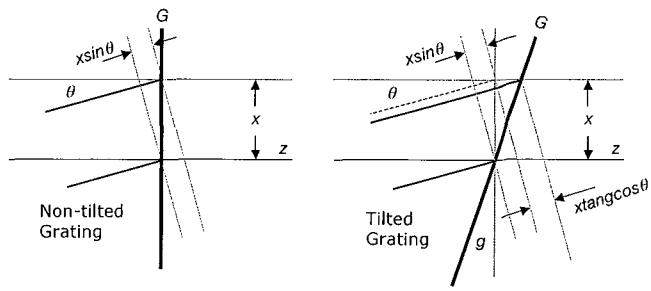

Fig. 3. Computing the grating phase. This is a side-view schematic of a plane wave propagating at angle θ striking a diffraction grating in non-tilted (left) and tilted (right) configurations. For the tilted case to the right, the ray that would be used for the non-tilted case is shown with dashed lines. See section 2.B for an in-depth description.

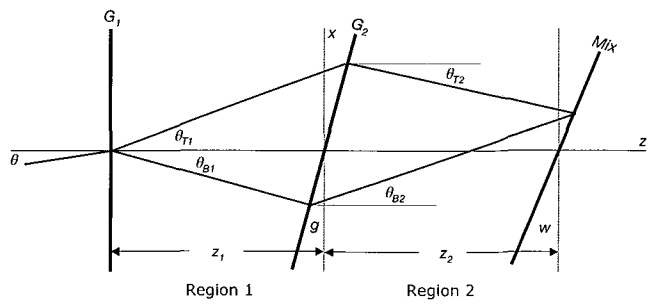

Fig. 4. Two-grating interferometer nomenclature. This is a side-view schematic of the two-grating interferometer and describes the nomenclature used throughout this paper for distances, angles, regions, etc.

Table 1. Tracking the propagation phase

Beam	Propagation Phase
T1	$\frac{2\pi}{\lambda}(z_1 + x\tan g)\cos\theta_{T1}$
B1	$\frac{2\pi}{\lambda}(z_1 + x\tan g)\cos\theta_{B1}$
T2	$\frac{2\pi}{\lambda}(z_2 - x\tan g + x\tan w)\cos\theta_{T2}$
B2	$\frac{2\pi}{\lambda}(z_2 - x\tan g + x\tan w)\cos\theta_{B2}$

Table 2. Tracking the grating phase

Beam	Grating Phase
T1	$\frac{2\pi}{\lambda}x(\sin\theta_{T1} - \sin\theta)$
B1	$\frac{2\pi}{\lambda}x(\sin\theta_{B1} - \sin\theta)$
T2	$\frac{2\pi}{\lambda}x(\sin\theta_{T2} - \sin\theta_{T1}) + \frac{2\pi}{\lambda}x\tan g(\cos\theta_{T2} - \cos\theta_{T1})$
B2	$\frac{2\pi}{\lambda}x(\sin\theta_{B2} - \sin\theta_{B1}) + \frac{2\pi}{\lambda}x\tan g(\cos\theta_{B2} - \cos\theta_{B1})$

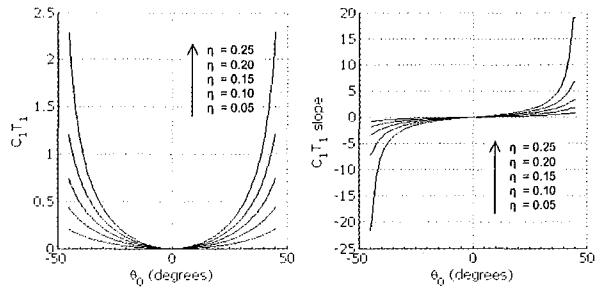

Fig. 5. Plots of the C_1T_1 product (left) and it's derivative with respect to. θ (right) for for several values of $\eta \equiv \lambda f_1 \in [0.05, 0.25]$ with $-45 < \theta < 45$ degrees.